






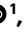
Mediterranean summer marine heatwaves triggered by weaker winds under subtropical ridges

Received: 28 October 2024

Accepted: 2 July 2025

Published online: 14 August 2025



Giulia Bonino ^{1,3}✉, Ronan McAdam ^{1,3}✉, Panos Athanasiadis ¹,
Leone Cavicchia ¹, Regina R. Rodrigues ², Enrico Scoccimarro ¹,
Stefano Tibaldi¹ & Simona Masina ¹

Marine heatwaves, extended periods of elevated sea surface temperature, impact society and ecosystems, and deeper understanding of their drivers is needed to predict and mitigate adverse effects. These events can be particularly severe in the Mediterranean Sea during the summer although the factors that control their occurrence and duration are not fully known. Here we use a comprehensive multi-decadal macroevent dataset and a cluster analysis to investigate the atmospheric dynamics preceding the largest summer marine heatwaves in the Mediterranean Sea. Our study identifies the favourable conditions leading up to marine heatwave peaks and reveals that their main synoptic cause in the Mediterranean Sea is the combined effect of persistent subtropical anticyclonic ridges and associated weakening of prevailing wind systems. When persistent subtropical ridges are established over the region, the resulting decrease in wind speeds causes a substantial reduction in latent heat loss to the atmosphere, which accounts for over 70% of the total heat flux in affected regions. This reduction, combined with a moderate increase in short-wave radiation, generates and intensifies marine heatwaves. This synergistic relationship represents a key mechanism that is critical for skilfully predicting such atmospheric circulation patterns and realistically simulating their impacts on the marine environment.

Marine heatwaves (MHWs) are prolonged periods of anomalously high sea surface temperatures (SSTs) that substantially impact marine ecosystems and climate¹. The Mediterranean Sea is particularly susceptible to these events due to the interplay of air–sea heat fluxes and local oceanographic processes^{2–4}, with mass-mortality events strongly linked to their occurrence⁵. Both long-term warming and interannual variability, exacerbated by climate change, contribute to the increasing frequency, intensity and duration of MHWs in the region⁶. This trend is consistent with global observations, as MHWs have become more frequent, intense and long-lasting worldwide⁷. The Mediterranean Sea, identified as a climate change hotspot⁸, is experiencing warming

rates exceeding global averages⁹, making it particularly vulnerable to extreme events such as MHWs. Notable Mediterranean Sea MHWs include those of 2003^{10,11}, 2007¹² and 2020^{13,14} and the exceptional 2022 event^{15,16}. These events have had severe ecological and economic consequences, including mass mortality of marine species¹⁷, shifts in species distributions¹⁸ and impacts on fisheries and aquaculture¹⁹. The cascading effects of MHWs can persist long after the thermal anomalies have dissipated, highlighting the need for improved understanding and prediction of these events.

An understanding of the synoptic large-scale drivers of Mediterranean MHWs, a necessary component to evaluating event

¹CMCC Foundation - Euro-Mediterranean Center on Climate Change, Bologna, Italy. ²Federal University of Santa Catarina, Florianópolis, Brazil. ³These authors contributed equally: Giulia Bonino, Ronan McAdam. ✉e-mail: giulia.bonino@cmcc.it; ronan.mcadam@cmcc.it

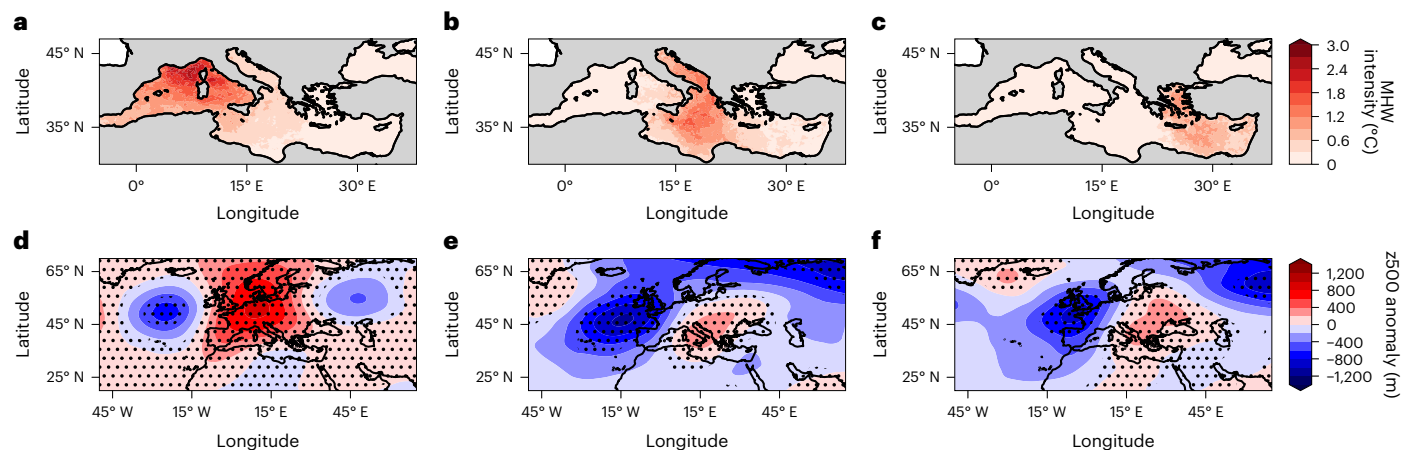


Fig. 1 | MHW cluster patterns and atmospheric circulation patterns during the MHW onset. a–c, MHW cluster intensity from ESA CCI SST for the three Mediterranean Sea clusters: WMed (a), CMed (b) and EMed (c). **d–f,** Corresponding ERA5 z500 anomaly composites during the onset period for

the three Mediterranean Sea clusters: WMed (d), CMed (e) and EMed (f). Black points in d–f denote statistically significant anomalies (Methods). The anomalies are calculated against the full study period (1982–2022).

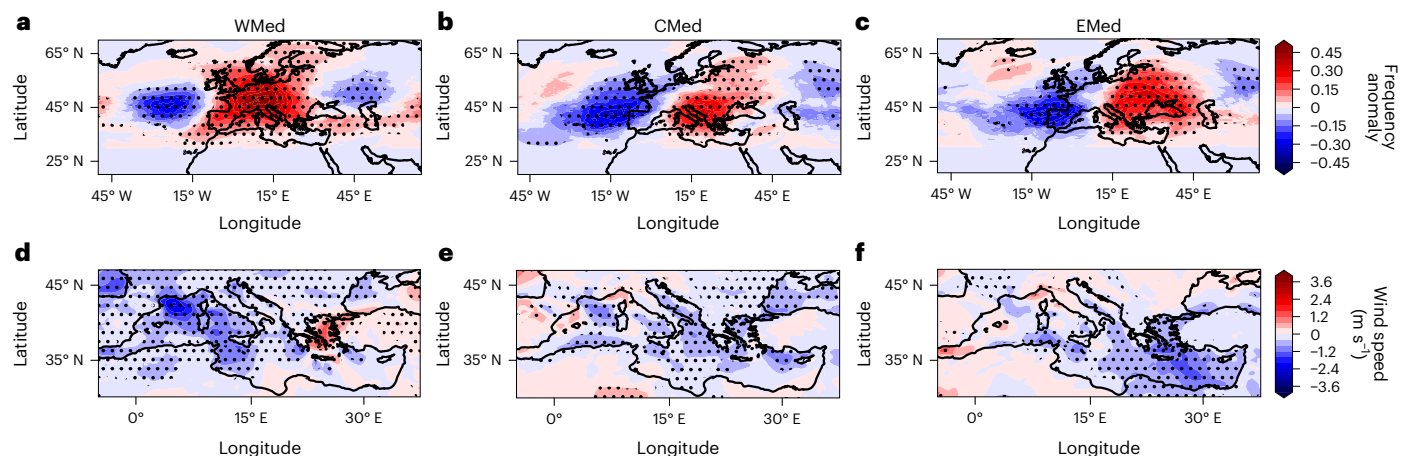


Fig. 2 | STR frequencies and wind-speed anomalies during MHW onset. a–f, Composites of anomalies of STR (a–c) and blocking (d–f) frequency indices, derived from ERA5 z500 data, for the WMed (a,d), CMed (b,e) and EMed (c,f) clusters (Fig. 1a). Black points denote statistically significant anomalies (Methods). The anomalies are calculated against the full study period (1982–2022).

predictability, is still lacking since previous studies have examined only atmospheric conditions associated with individual MHWs in the Mediterranean Sea^{10,13,16}. Denaxa et al.² identified air–sea heat fluxes as the primary driver of MHWs in the Mediterranean, finding the latent heat flux to be the major heat-flux component. Such anomalies in the Mediterranean are probably linked to regional synoptic atmospheric circulation patterns that govern the onset of MHWs. Garfinkel et al.²⁰ identified robust precursors of atmospheric heatwaves in the eastern Mediterranean present 7–10 days before onset, demonstrating that horizontal temperature advection in the days before the extreme is the cause of the heatwave, particularly through a weakening of the Etesian winds that would otherwise advect relatively cool maritime air inland. High-pressure systems and anticyclonic conditions enhance solar radiation and minimize heat loss from the Mediterranean Sea to the atmosphere¹⁶. Common drivers of atmospheric heatwaves, however, have been studied in more detail. For example, atmospheric blocking, the manifestation of a persistent high-pressure system, is a known driver of atmospheric heatwaves over central to northern Europe²¹. These high-pressure systems sometimes initially appear as anticyclonic intrusions from the subtropics^{22,23}, formally known as subtropical ridges (STRs). STRs have also been linked to the occurrence of atmospheric heatwaves over Mediterranean countries,

further south than blocking-related events^{20,24–26}. While STRs are specifically extensions of the subtropical high-pressure belt that protrude northward, atmospheric blocking displays closed circulation patterns²⁷. As STRs are also known to influence MHWs around Australia²⁸, in this study we examine their role in the formation of these events in the Mediterranean.

Our work uses a comprehensive multi-decadal dataset of multiple Mediterranean MHW macroevents²⁹, built from the European Space Agency (ESA) Climate Change Initiative (CCI) SST satellite dataset³⁰, to identify common atmospheric conditions and circulation patterns across the basin conducive to MHWs, as opposed to previous studies, which have examined atmospheric conditions associated with individual events in the Mediterranean Sea^{10,13,16}. We analyse composite anomalies of wind, geopotential height and atmospheric heat fluxes, as provided by the European Centre for Medium-Range Weather Forecasts Reanalysis v5 (ERA5) atmospheric reanalysis³¹, to identify conditions favouring MHW development in three representative sub-basins (west, central and east). Our results explicitly identify the role of persistent anticyclonic STRs in Mediterranean MHW, using a multi-event dataset. The identification of the source of predictability as one with a short-term window has crucial implications for improving the accuracy of forecasts and enhancing the effectiveness of impact

Table 1 | LR and co-occurrence statistics for MHW formation

	WMed	CMed	EMed
Likelihood ratios			
LR for STR+NegWind	4.35 ^a	4.29 ^a	4.81 ^a
LR for STR only	0.69	0.98	0.57
LR for NegWind only	0.78	0.98	1.27
<i>P</i> -value LR for STR+NegWind	9.71×10^{-67a}	1.87×10^{-30a}	3.73×10^{-26a}
Co-occurrence			
MHWs with STR+NegWind (%)	63.3	46.4	41.3
MHWs with STR only (%)	28.6	37.1	31.3
MHWs with NegWind only (%)	4.1	5.2	5.0
MHWs with neither (%)	4.1	11.3	22.5

All statistical tests are based on two-sided *t* tests. ^aStatistically significant at $P < 0.01$.

mitigation strategies, in this region and others potentially subject to MHWs determined by STRs.

The occurrence of persistent STRs and weakened winds in relation to MHWs

In this Article, we use hierarchical clustering analysis to group summer (May–June–July–August) MHWs that extend beyond 100,000 km² for the period of 1982–2022 (Methods). These extensive MHWs have occurred in the western, central and eastern sub-basins of the Mediterranean Sea (WMed, CMed and EMed, respectively), with SST anomalies reaching up to 3 °C during the onset period (Fig. 1a–c, respectively). The MHWs are associated with anticyclonic (clockwise) atmospheric circulation depicted by positive anomalies of geopotential height at 500 hPa (z500 anomalies; red shading in Fig. 1d–f). This suggests the presence of stable, high-pressure systems that probably enhance the persistence and intensity of MHWs. Cyclonic (anticlockwise) centres represented by negative z500 anomalies (blue shading in Fig. 1d–f) associated with low-pressure centres surround the anticyclonic centres, suggesting the presence of a coherent wave-train pattern. Thus, we conclude that atmospheric conditions conducive to MHWs are part of a broader-scale atmospheric circulation dynamic, where alternating high- and low-pressure systems propagate throughout the Mediterranean basin.

Atmospheric circulation patterns associated with atmospheric and marine heatwaves³², similar to those identified in Fig. 1, are often attributed to blocking, although sometimes erroneously²¹. Moreover, previous studies have identified z500 anomalies during individual MHWs^{6,10,13,16,33}, without either attributing them to specific processes or using dedicated indices for blocking and ridges. While STRs are common over the Mediterranean, with climatological frequencies between 0.5 (that is, one every 2 days in the summer) and 0.8 for all the three clusters, blocking is extremely rare, with frequencies below 0.02 (Extended Data Fig. 1). Here we explicitly show that anticyclonic centres linked to MHWs in the Mediterranean Sea are associated with persistent STRs (Fig. 2). The occurrence of STRs is significantly more frequent, with respect to their climatology (Extended Data Fig. 1), over the regions undergoing MHWs during their onset period (Fig. 2a–c). The rate of occurrence rises to one every day, implying the presence of a persistent ridge. Positive anomalies of STR occurrence are flanked east and west by negative anomalies, indicative of a wavy flow pattern persisting over the MHW regions⁶. This result is consistent across all clusters, with STR patterns simply shifting longitudinally (eastwards) and aligning with the cluster locations.

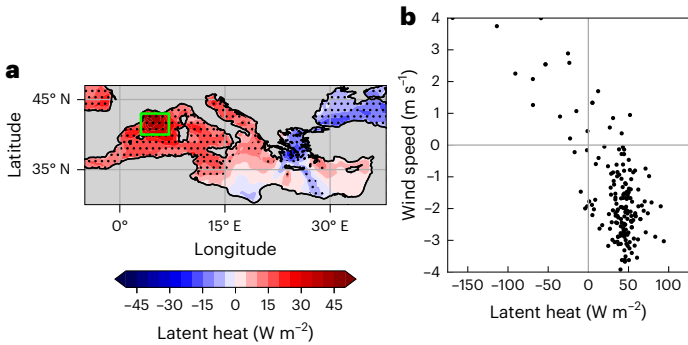


Fig. 3 | Atmospheric conditions inducing MHW onset. a, ERA5 latent heat anomaly composites for WMed onset. **b**, Respective daily anomalies of ERA5 latent heat and wind speed during the onset period. Values are area averages inside the green frame shown in **a** and exhibit a linear correlation equal to -0.71 . Black points in **a** denote statistically significant anomalies (Methods). The anomalies are calculated against the full study period (1982–2022). Latent heat is positive towards the ocean.

Moreover, the critical factor we identify is not merely the presence of STRs but their persistence and co-occurrence with reduced wind conditions (Fig. 2d–f). To quantify this relationship, we calculated likelihood ratios (LRs), which provide a metric for evaluating the strength of association between atmospheric conditions and MHW occurrence (Table 1). Our analysis reveals evidence for the combined impact of STRs and reduced wind speed. When persistent STRs and negative wind anomalies (NegWind) co-occur, the likelihood ratio for MHW occurrence rises to 4.35, 4.29 and 4.81 for the WMed, CMed and EMed, respectively, with respect to the background probability (Table 1). This means that MHWs are approximately 4–5 times more likely to form when both conditions are present simultaneously compared with the background probability. These associations are highly statistically significant ($P < 1 \times 10^{-25}$ for all clusters). Importantly, the likelihood ratios for STR only (without wind reduction) and wind reduction only (without STRs) are much lower—often below or only slightly above 1.0 (Table 1). This indicates that neither condition alone substantially increases MHW probability. A substantial portion of Mediterranean MHWs occur during periods with both STRs and reduced wind conditions: 41.3%, 46.4% and 63.3% for the EMed, CMed and WMed, respectively (Table 1). This is particularly striking considering that the STR + NegWind condition itself occurs during only 8.6%, 10.8% and 14.6% of all days in the EMed, CMed and WMed, respectively.

MHWs caused by the anomalous surface heat fluxes associated with STRs

Increased STR occurrence corresponds with significant decreases in wind speed and reduction of latent heat loss, which are primary candidates for heat-flux increase into the ocean, during the MHW onset (Fig. 3 for WMed; Extended Data Figs. 2 and 3 for CMed and EMed, respectively). The weakening or switching-off of the Mistral (strong northwesterlies over the Gulf of Lion; Fig. 2; Extended Data Fig. 4 for wind climatologies) corresponds to WMed events, and a weakening of the Etesians (northerlies over the Aegean Sea; Extended Data Fig. 3b) corresponds to EMed events. Reduction of wind speeds (up to -4 m s^{-1} in the Gulf of Lion; Fig. 3b) inhibits evaporation, which leads to reduced latent heat loss by the ocean (positive anomalies up to 100 W m^{-2} in the Gulf of Lion; Fig. 3a). The latent heat signals are also confirmed by observational data (from Objectively Analyzed Air–Sea Fluxes for the Global Oceans³⁴; Methods and Extended Data Fig. 5).

Our analysis reveals a strong anti-correlation between wind-speed anomalies and latent heat anomalies during the onset period, with regression coefficients (*r*) of -0.71 , -0.68 and -0.73 for the WMed, CMed and EMed clusters, respectively (Fig. 3b and Extended Data

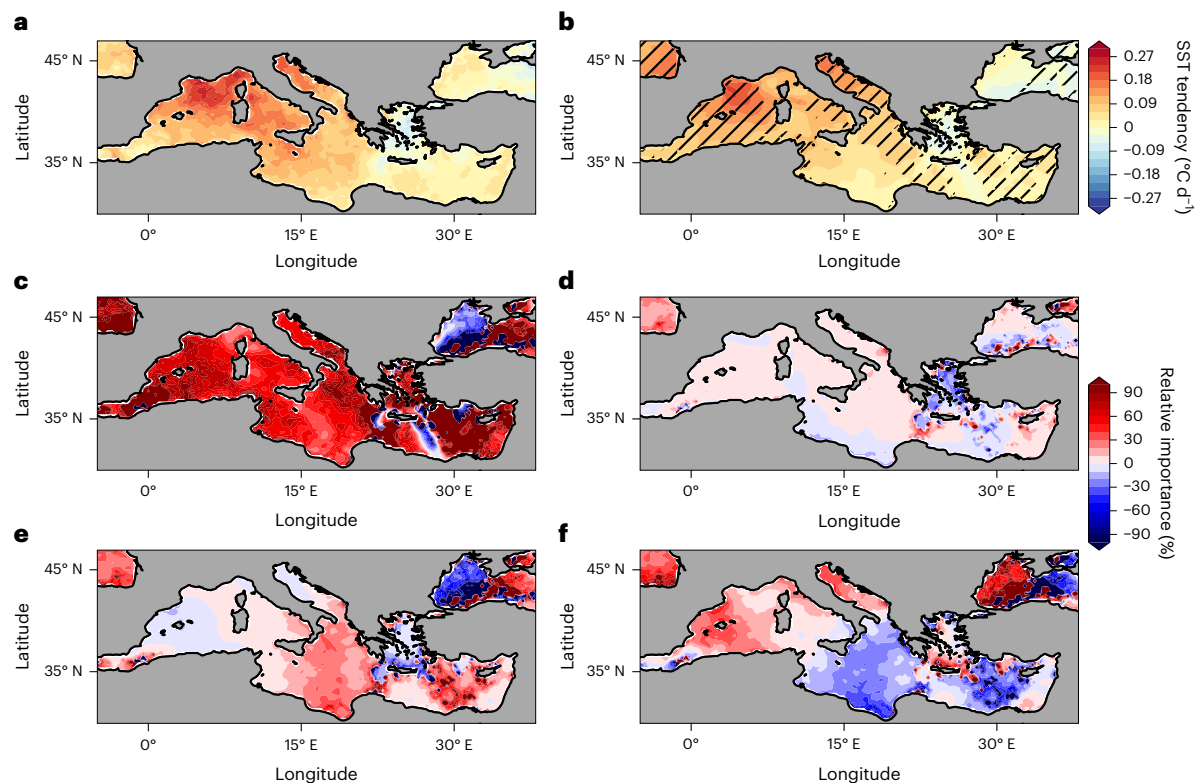


Fig. 4 | SST tendency and atmosphere–sea heat-flux components during MHW onset. a, Composites of ESA CCI SST tendency for WMed. **b**, Equivalent SST tendency of total fluxes for WMed. **c–f**, Relative importance with respect to the SST tendency (**a**) of the four flux components from ERA5: latent (**c**), sensible

(**d**), net long-wave radiation (**e**) and net short-wave radiation (**f**). Hatching in **b** identifies where the equivalent flux tendency explains more than 70% of the SST tendency in **a**. The anomalies are calculated against the full study period (1982–2022).

Figs. 2b and 3b). This mechanistic relationship is consistent with our statistical findings in Table 1, which show that neither STRs nor wind reduction alone significantly increase MHW probability. The combined effect of atmospheric circulation (STRs) and its surface manifestation (reduced winds) is essential for MHW formation, with the physical connection being the reduced evaporative cooling that allows ocean warming. In the areas of maximum MHW intensity, the spatial correspondence between latent heat anomalies and wind anomalies is particularly strong (Fig. 3 and Extended Data Figs. 2 and 3).

The spatial patterns of SST tendency (Fig. 4a) before the MHW peak and the equivalent tendency derived from the atmosphere–sea heat fluxes (Fig. 4b) largely coincide: for WMed, maximum values are located across the northwest part of the basin and in the Adriatic Sea. Crucially, the magnitudes (for example, up to 0.3 °C d^{-1} in the Gulf of Lion) are also nearly identical. Indeed, more than 70% of the SST tendency is explained (Fig. 4b hatching) by the total heat-flux tendencies. Therefore, the non-atmosphere processes roughly account for the remaining 30%. Latent heat is found to be the major contributor to the flux-related heat transport, accounting for over 80% of the SST tendency in the areas of interest (Fig. 4c–f and Extended Data Figs. 6 and 7). This confirms that the reduction in wind speed is the primary physical mechanism influencing SST through decreased evaporative cooling. Anomalies of sensible heat, net short-wave and long-wave radiation, are in places significantly different from average conditions (Extended Data Fig. 8), but they generally provide a minor contribution to the SST tendency (Fig. 4d–f). However, there are exceptions, for example, long-wave radiation in the central part of the basin during WMed events and the short-wave radiation over the Gulf of Lion. By contrast, the contribution of sensible heat is largely negligible across the basin. Similar results are found for the CMed (Extended Data Fig. 6) and EMed (Extended Data Fig. 7) clusters.

Implications for predictability and modelling

This work has identified the combined effect of STRs and associated wind reduction as the key mechanism leading to the development of summer MHWs across the Mediterranean basin. Here we use an event-based dataset covering the Mediterranean Sea over the satellite data period (1982–2022) to evaluate the role of this synergistic relationship.

Our analysis demonstrates that STRs correspond to the wind and heat-flux conditions necessary to induce MHWs, with wind reduction under STRs causing decreased evaporative cooling as the primary physical mechanism, accompanied by a more moderate and less-widespread increase in short-wave radiation. The study by Garfinkel et al.²⁰ found that atmospheric heatwaves over land areas in the eastern Mediterranean co-occur with warm SSTs and are preceded by warm SSTs farther west. Their analysis revealed that horizontal temperature advection due to weakened Etesian winds is the proximate cause of atmospheric heat extremes, which aligns with our findings that reduced wind speeds under STRs drive MHWs through decreased evaporative cooling. Similarly, Denaxa et al.² investigated the role of air–sea heat exchange during MHWs in the Mediterranean and found that latent heat flux emerges as the major heat-flux component in the SST evolution across all seasons, with air–sea heat flux being the major driver of MHW onset phases. Our results complement and extend these findings by identifying the specific atmospheric circulation pattern (persistent STRs) that drives the reduction in wind speeds and subsequently the anomalous latent heat flux that generates MHWs. Unlike in other regions (for example, the South Atlantic Ocean³⁵), atmospheric blocking does not play a role in Mediterranean summer MHW onset due to its rarity in this region. Instead, the Mediterranean is characterized by frequent STRs, and it is specifically their persistence and co-occurrence with reduced wind conditions that creates ideal conditions for MHW formation.

The combined effect of STRs and reduced winds therefore represents a potential source of predictability for MHWs. Persistent z500 anomalies extending past the subtropical belt are related to MHWs. The persistent STR index used here can act as an indicator for MHWs when combined with information on surface wind anomalies. Previous studies^{36,37} have also proposed indicators for local temperature extremes based on atmospheric circulation. Indicators of potential predictors of extreme events are applied in forecasting, especially in the emerging field of machine-learning-based forecasting. Machine-learning forecasts of MHWs in particular require information on atmospheric conditions^{38,39}. Therefore, we propose the combined STR–wind–reduction pattern as an indicator of MHWs across the Mediterranean basin.

However, STR–wind reduction provides only a small window of predictability of approximately less than 10 days, similar to blocking^{40,41}. The next step is to understand what drives the excitation, at subseasonal to seasonal timescales, of STRs at a given longitude to boost the window of predictability. The atmospheric circulation anomalies associated with the MHW clusters closely resemble a wave train, with depressions on either side of the high pressure³⁵, suggesting a role of hemisphere-scale dynamics. For example, similar composite analyses have detected heightened summer 2 m temperature and SST anomalies in Europe during instances of North Atlantic depressions^{6,42}. The genesis of these depressions/wave trains may influence the propensity of STR excitation in a season at particular longitudes, which in turn may shed light on the predictability of Mediterranean MHWs. Furthermore, current seasonal forecasts of MHWs in the Mediterranean area are often unreliable^{43,44}, possibly due to their inability to correctly represent the occurrence of STRs. Our work highlights previously unidentified processes that are essential for accurately representing Mediterranean MHWs. These results are critical for improving forecast systems and Earth system models, representing a key step towards effective early-warning and mitigation strategies in the basin.

Online content

Any methods, additional references, Nature Portfolio reporting summaries, source data, extended data, supplementary information, acknowledgements, peer review information; details of author contributions and competing interests; and statements of data and code availability are available at <https://doi.org/10.1038/s41561-025-01762-9>.

References

- Hobday, A. J. et al. A hierarchical approach to defining marine heatwaves. *Prog. Oceanogr.* **141**, 227–238 (2016).
- Denaxa, D., Korres, G., Bonino, G., Masina, S. & Hatzaki, M. in *Copernicus Ocean State Report (OSR8)* 8th edn (eds von Schuckmann, K. et al.) Ch. 3.3 (State of the Planet. 2024).
- Darmaraki, S., Somot, S., Sevault, F. & Nabat, P. Past variability of Mediterranean Sea marine heatwaves. *Geophys. Res. Lett.* **46**, 9813–9823 (2019).
- Darmaraki, S. et al. Marine heatwaves in the Mediterranean Sea: a literature review. *Mediterr. Mar. Sci.* **25**, 586–620 (2024).
- Garrabou, J. et al. Marine heatwaves drive recurrent mass mortalities in the Mediterranean Sea. *Glob. Change Biol.* **28**, 5708–5725 (2022).
- Simon, A., Pires, C., Frölicher, T. L. & Russo, A. Long-term warming and interannual variability contributions to marine heatwaves in the Mediterranean. *Weather Clim. Extrem.* **42**, 100619 (2023).
- Oliver, E. C. J. et al. Longer and more frequent marine heatwaves over the past century. *Nat. Commun.* **9**, 1324 (2018).
- Giorgi, F. Climate change hot-spots. *Geophys. Res. Lett.* <https://doi.org/10.1029/2006GL025734> (2006).
- Cramer, W. et al. Climate change and interconnected risks to sustainable development in the Mediterranean. *Nat. Clim. Change* **8**, 972–980 (2018).
- Olita, A. et al. Effects of the 2003 European heatwave on the Central Mediterranean Sea: observations and model analysis. *J. Geophys. Res. Oceans* <https://doi.org/10.1029/2006JC003998> (2007).
- Sparnocchia, S., Schiano, M. E., Picco, P., Bozzano, R. & Cappelletti, A. The anomalous warming of summer 2003 in the surface layer of the Central Ligurian Sea (Western Mediterranean). *Ann. Geophys.* **24**, 443–452 (2006).
- Mavrakis, E. & Tsiros, I. X. Marine heatwave in the eastern Mediterranean Sea during summer 2007. *Theor. Appl. Climatol.* **133**, 1031–1042 (2018).
- Ibrahim, O., Mohamed, B. & Nagy, H. Spatial variability and trends of marine heat waves in the eastern Mediterranean Sea over 39 years. *J. Mar. Sci. Eng.* **9**, 643 (2021).
- Denaxa, D., Korres, G., Sotiropoulou, M. & Perivoliotis, L. Extreme marine heatwave in the eastern Mediterranean in May 2020. *J. Operat. Oceanogr.* **15**, s192–s198 (2022).
- McAdam, R., Bonino, G., Clementi, E. & Masina, S. in *Copernicus Ocean State Report (OSR8)* 8th edn (eds Schuckmann, K. et al.) Ch. 4.1 (State of the Planet, 2024).
- Marullo, S. et al. The longest marine heatwave in the Mediterranean Sea: the exceptional 2022 event. *Nat. Commun.* **14**, 257 (2023).
- Garrabou, J. et al. Mass mortality in northwestern Mediterranean rocky benthic communities: effects of the 2003 heat wave. *Glob. Change Biol.* **15**, 1090–1103 (2009).
- Vergés, A. et al. Tropical rabbitfish and the deforestation of a warming temperate sea. *J. Ecol.* **102**, 1518–1527 (2014).
- Sarà, G. et al. Impacts of climate change on Mediterranean marine ecosystems: the case of the great crested grebe (*Podiceps cristatus*). *Mar. Ecol. Prog. Ser.* **332**, 247–253 (2007).
- Garfinkel, C. I. et al. Precursors of summer heat waves in the eastern Mediterranean. *Q. J. R. Meteorol. Soc.* **50**, 3757–3773 (2024).
- Barriopedro, D., García-Herrera, R., Ordóñez, C., Miralles, D. G. & Salcedo-Sanz, S. Heat waves: physical understanding and scientific challenges. *Rev. Geophys.* **61**, e2022RG000780 (2023).
- Sousa, P. M., Trigo, R. M., Barriopedro, D., Soares, P. M. M. & Santos, J. A. European temperature responses to blocking and ridge regional patterns. *Clim. Dyn.* **50**, 457–477 (2018).
- Sousa, P. M. et al. Distinct influences of large-scale circulation and regional feedbacks in two exceptional 2019 European heatwaves. *Commun. Earth Environ.* **1**, 48 (2020).
- Sánchez-Benítez, A., Barriopedro, D. & García-Herrera, R. Tracking Iberian heatwaves from a new perspective. *Weather Clim. Extrem.* **28**, 100238 (2020).
- Lemus-Canovas, M., Insua-Costa, D., Trigo, R. M. & Miralles, D. G. Record-shattering 2023 spring heatwave in western Mediterranean amplified by long-term drought. *npj Clim. Atmos. Sci.* **7**, 25 (2024).
- Lhotka, O. & Kyselý, J. Three-dimensional analysis reveals diverse heat wave types in Europe. *Commun. Earth Environ.* **5**, 323 (2024).
- Woollings, T. et al. Blocking and its response to climate change. *Curr. Clim. Change Rep.* **4**, 287–300 (2018).
- Gregory, C. H., Holbrook, N. J., Marshall, A. G. & Spillman, C. M. Sub-seasonal to seasonal drivers of regional marine heatwaves around Australia. *Clim. Dyn.* **62**, 6599–6623 (2024).
- Bonino, G., Masina, S., Galimberti, G. & Moretti, M. Southern Europe and western Asian marine heatwaves (SEWA-MHWs): a dataset based on macroevents. *Earth Syst. Sci. Data* **15**, 1269–1285 (2023).
- Merchant, C. J. et al. Satellite-based time-series of sea-surface temperature since 1981 for climate applications. *Sci. Data* **6**, 223 (2019).

31. Hersbach, H. et al. The ERA5 global reanalysis. *Q. J. R. Meteorol. Soc.* **146**, 1999–2049 (2020).
32. Feudale, L. & Shukla, J. Influence of sea surface temperature on the European heat wave of 2003 summer. Part I: an observational study. *Clim. Dyn.* **36**, 1691–1703 (2011).
33. Guinaldo, T., Voldoire, A., Waldman, R., Saux Picart, S. & Roquet, H. Response of the sea surface temperature to heatwaves during the France 2022 meteorological summer. *Ocean Sci.* **19**, 629–647 (2023).
34. Yu, L. & Weller, R. A. Objectively analyzed air–sea heat fluxes for the global ice-free oceans (1981–2005). *Bull. Amer. Meteor. Soc.* **88**, 527–540 (2007).
35. Rodrigues, R. R., Taschetto, A. S., Sen Gupta, A. & Foltz, G. R. Common cause for severe droughts in South America and marine heatwaves in the South Atlantic. *Nat. Geosci.* **12**, 620–626 (2019).
36. Harpaz, T., Ziv, B., Saaroni, H. & Beja, E. Extreme summer temperatures in the East Mediterranean—dynamical analysis. *Int. J. Climatol.* **34**, 849–862 (2014).
37. Jansa, A. et al. Extension of summer climatic conditions into spring in the western Mediterranean area. *Int. J. Climatol.* **37**, 1938–1950 (2017).
38. Giamalaki, K., Beaulieu, C. & Prochaska, J. Assessing predictability of marine heatwaves with random forests. *Geophys. Res. Lett.* **49**, e2022GL099069 (2022).
39. Bonino, G., Galimberti, G., Masina, S., McAdam, R. & Clementi, E. Machine learning methods to predict sea surface temperature and marine heatwave occurrence: a case study of the Mediterranean Sea. *Ocean Sci.* **20**, 417–432 (2024).
40. Tibaldi, S. & Molteni, F. On the operational predictability of blocking. *Tellus A* **42**, 343–365 (1990).
41. Matsueda, M. Blocking predictability in operational medium-range ensemble forecasts. *Sola* **5**, 113–116 (2009).
42. D’Andrea, F. et al. Summer deep depressions increase over the eastern North Atlantic. *Geophys. Res. Lett.* **51**, e2023GL104435 (2024).
43. McAdam, R., Masina, S. & Gualdi, S. Seasonal forecasting of subsurface marine heatwaves. *Commun. Earth Environ.* **4**, 225 (2023).
44. De Boissésou, E. & Balmaseda, M. A. Predictability of marine heatwaves: assessment based on the ECMWF seasonal forecast system. *Ocean Sci.* **20**, 265–278 (2024).

Publisher’s note Springer Nature remains neutral with regard to jurisdictional claims in published maps and institutional affiliations.

Open Access This article is licensed under a Creative Commons Attribution 4.0 International License, which permits use, sharing, adaptation, distribution and reproduction in any medium or format, as long as you give appropriate credit to the original author(s) and the source, provide a link to the Creative Commons licence, and indicate if changes were made. The images or other third party material in this article are included in the article’s Creative Commons licence, unless indicated otherwise in a credit line to the material. If material is not included in the article’s Creative Commons licence and your intended use is not permitted by statutory regulation or exceeds the permitted use, you will need to obtain permission directly from the copyright holder. To view a copy of this licence, visit <http://creativecommons.org/licenses/by/4.0/>.

© The Author(s) 2025

Methods

Datasets used

ERA5, the multi-decadal three-dimensional reanalysis of the atmosphere at 0.25° horizontal resolution at the surface³¹, is used to produce regional-scale composites of atmospheric conditions. The following variables are used: geopotential height at 500 hPa, potential temperature at the tropopause (−2 PV units), horizontal components of winds at 10 m, mean surface values of latent and sensible heat, and long-wave and short-wave radiation fluxes. Objectively Analyzed Air–Sea Fluxes for the Global Oceans, specifically the daily 1° satellite-derived analysis, is also used, to validate the latent heat flux of ERA5.

For our study, we used an MHW dataset, which provides a detailed record of MHW macroevents and their characteristics across the southern European and western Asian (SEWA) basins from 1981 to 2016, named the SEWA–MHW dataset as described by Bonino et al.²⁹. This dataset, derived from the ESA CCI SST v2.1 dataset³⁰, identifies MHWs at each 5 × 5 km grid point and applies connected component analysis to group spatiotemporally linked MHWs into larger macroevents while maintaining high-resolution data. To extend the temporal coverage, we included daily SST data from 2017 to 2021, obtained from the Copernicus Climate Data Store (last accessed 12 June 2025). This extended dataset, covering 2017 to 2022, is generated at level 4 by the Copernicus Climate Change Service and builds on the ESA CCI SST dataset. MHWs in the SST dataset are first detected relative to a time-varying baseline climatology, calculated along the full study period (see ref. 29 for more details), which accounts for both trends and seasonal variability. This approach adjusts for shifts in the climate mean state, isolating the interannual variability of the signal⁴⁵. Second, connected component analysis aggregates MHWs that are spatially and temporally linked, transitioning from a grid-cell-based dataset to an event-based dataset without sacrificing the high-resolution grid-cell information. This method provides a detailed temporal evolution of MHWs at the basin scale. By using this dataset, we ensured consistency and comparability with other MHW studies, adhering to recent recommendations for a standardized MHW definition and spatial considerations^{46,47}.

MHW macroevent detection methodology

We used hierarchical clustering to group the summer (May–June–July–August) macroevents, following the methodology of Bonino et al.²⁹. This enabled us to effectively characterize and analyse the largest MHW macroevents, identifying typical spatial patterns of summer MHWs over the SEWA basins. From the 68,900 identified macroevents, we focused on those with the largest area extensions, retaining 123 macroevents exceeding 100,000 km². For each macroevent, we extracted daily mean intensity maps and averaged them to produce a single event map. Using an agglomerative hierarchical clustering algorithm based on cosine distances⁴⁸, we identified three clusters over the Mediterranean Sea. As expected, the spatial patterns closely match those in ref. 29 for the Mediterranean Sea, except for the number of events in each cluster. Cluster 1, spanning the western Mediterranean and Adriatic seas, contained 26 macroevents. Cluster 2 centred on the Adriatic Sea and included 18 macroevents; cluster 3, centred around the Aegean Sea, included 14 macroevents. In this study, the clusters are referred to as WMed, CMed and EMed, respectively.

To identify the peak of each macroevent, we determined the time at which the MHW experienced its first and fastest growth in terms of area. This was done by analysing the time-series data of MHW area, focusing on the period when the area expanded most rapidly. The area is defined as the sum of the pixels experiencing MHWs on each day. To account for short-term fluctuations, we smoothed the time-series data using a running mean with a time window proportional to the event duration. Then we calculated the rate of change in area to pinpoint the peak growth phase. The date corresponding to this peak was recorded for each macroevent, ensuring a consistent identification of the critical

growth phase across all events. We chose the 5-day period before the peak as the onset period of MHWs.

Atmospheric circulation patterns

STRs are defined as extensions of the subtropical belt (STB) beyond its zonal mean latitude (see fig. 1 in ref. 49; Extended Data Fig. 1a). They are meanders of westerly flow that redirect atmospheric circulation over the Mediterranean region and farther poleward, and are either short-lived stand-alone phenomena or the first stage in the life cycle of blocks. To identify STRs, the following steps have been recommended⁴⁹. First, a high-pressure zone is defined as a region where the z500 is greater than the hemisphere-wide average over the previous 15 days (to account for long-term trends and seasonal cycle). Second, the STB is defined as the minimum latitude of the high-pressure zone, splitting the hemisphere into two domains. The STB is therefore seasonally varying and, in the summer, reaches latitudes of 40° and thus beyond the extent of the Mediterranean Sea. Finally, STRs are defined where positive anomalies of z500 occur polewards of the STB⁴⁹. Here we choose to modify the second step of the definition by imposing a fixed definition of the STB as 30° N to identify ridges that cover the Mediterranean Sea. The STR indices used here are two-dimensional, daily and impose no minimum duration.

Atmospheric blockings, like STRs, are also interruptions/redirections of westerly flow, but the key difference from STRs is that blocks are closed anticyclonic features that trap air masses (see fig. 1 in ref. 49). STRs that develop a closed anticyclonic flow at their core and, once unstable, undergo wave-breaking, become atmospheric blocking, completely separating the anticyclonic flow from the STB. There are many competing definitions for blocks, with studies proposing definitions based on different metrics of atmospheric circulation, or identifying more stages in the life cycle of blocks. Here we use positive anomalies of potential temperature in the tropopause (2 PV units) (ref. 50) to identify anticyclonic features that have undergone wave-breaking and persist for 5 days or longer, a definition previously used for detection of MHW drivers³⁵. We define boxes with dimensions of 15° latitude by 5° longitude to both the south and north of each central location. The potential temperature at 2 PV is averaged within these defined areas. We calculate a large-scale measure of the meridional potential temperature gradient by subtracting the average temperature in the southern box from that in the northern box. Positive differences for at least four consecutive days identify a wave-breaking event.

In this study, we adopt the terminology of STRs as defined in previous literature⁴⁹. It is important to distinguish these STRs from omega blocks or other blocking patterns. While they may appear similar in some respects, STRs are specifically extensions of the subtropical high-pressure belt that protrude northward, whereas omega blocks are characterized by a distinct omega-shaped closed circulation pattern²⁷.

Composites of atmospheric conditions are calculated by averaging the values over the onset period. Statistical significance of composite anomalies is determined with bootstrapping; 1,000 random samples, with a size equal to that of the composite samples (the number of onset days specific to each cluster), are taken from the months May to August and used to create a distribution of composites. The composites of MHW onset conditions are considered statistically significant if they fall above the 95th percentile of the distribution of random samples.

Event likelihood analysis

To robustly analyse the relationship between STRs, wind conditions and MHWs, we developed three specific indices:

- (1) **Persistent STR Index (STR).** We identified persistent STRs by requiring the presence of an STR system for five consecutive days within the defined box regions (shown in green in Fig. 3 and Extended Data Figs. 2 and 3) for each cluster. This persistence criterion is crucial as it filters out transient systems and focuses on the sustained atmospheric

patterns capable of influencing SSTs. The index is binary (1 if the condition is met, 0 otherwise) for each day in the time series.

- (2) Persistent Wind Anomaly Index (NegWind). For each cluster, we calculated the area-averaged wind-speed anomaly within the defined box regions. Negative values indicate lower-than-normal wind speeds. The presence of a negative speed anomaly has to be persistent for five consecutive days. The index is binary (1 if the condition is met, 0 otherwise) for each day in the time series.
- (3) MHW Onset Index (MHW). Our analysis specifically targets the MHW onset period, defined as the 5 days preceding the peak intensity of each event. We computed binary time series for onset days (1 if it is an onset day, 0 otherwise).

To quantify the relationship between these indices, we calculated LR, which provide a powerful metric for evaluating the strength of association between atmospheric conditions and MHW occurrence. The likelihood ratio is calculated as the ratio of the following probabilities (P):

$$LR = P(\text{MHW}|\text{Condition})/P(\text{MHW})$$

This metric directly quantifies how much more likely an MHW becomes under specific atmospheric conditions compared with its baseline probability. An LR of 1.0 indicates no association (that is, the condition does not affect MHW probability), while values greater than 1.0 indicate increased likelihood.

Heat-flux contribution analysis

The contribution of air–sea heat fluxes to the tendency in SST can be used to estimate whether MHWs are driven primarily by inflow of heat from the atmosphere. The equivalent SST change induced by the air–sea heat fluxes with time (t) can be estimated with:

$$\frac{d\text{SST}}{dt} = \frac{Q_h}{h \times \rho \times c_p}$$

assuming a fixed summer mixed-layer depth (h) of 5 m based on the climatological study of d’Ortenzio et al.⁵¹, a specific heat capacity of water (c_p) of 3,985 J kg^{−1} °C^{−1} and a density (ρ) of 1,025 kg m^{−3}. Q_h (positive downwards) represents the atmospheric heat-flux anomaly (either total or one of the four components) computed against the full study period. This is an approximation of the true value of SST tendency, which would include contributions from ocean advection and unresolved processes. The relative importance, or contribution to the total flux, of an atmospheric heat-flux anomaly component is its value as a percentage of the total flux component, allowing for negative contributions and values above 100%.

Data availability

The European Centre for Medium-Range Weather Forecasts (ECMWF) ERA5 reanalysis data are openly available at the Climate Data Store of the Copernicus Climate Change service (<https://cds.climate.copernicus.eu/>). OaFlux products are publicly accessible at <http://oafux.whoi.edu> (last accessed 12 June 2025). The SEWA–MHW macroevents dataset that consists of daily fields of MHW macroevents, their characteristics and basins from 1981 to 2016 is available via Zenodo (<https://doi.org/10.5281/zenodo.7153255>) (ref. 52). The SEWA–MHW extended dataset from 2017 to 2022 is based on European Space Agency Climate Change Initiative (ESA CCI) SST dataset v2.1 (ESA CCI SST, Merchant et al.³⁰, freely available in the CEDA catalogue⁵³ at <https://catalogue.ceda.ac.uk/uuid/62c0f97b1eac4e0197a674870afe1ee6>, for September 1981 to December 2016 and in the Copernicus CDS⁵⁴ at <https://cds.climate.copernicus.eu/datasets/satellite-sea-surface-temperature?tab=overview> for January 2017 to December 2021). The

dataset has been extended by running the codes detailed in ref. 29 and available via Zenodo (<https://doi.org/10.5281/zenodo.7153255>) (ref. 52). The Mediterranean macroevent data used to characterize the clusters in this paper are available via Zenodo (<https://doi.org/10.5281/zenodo.15690822>) (ref. 55).

Code availability

All figures were generated with the open-source software Python. The codes are available via Zenodo (<https://doi.org/10.5281/zenodo.15690822>) (ref. 55).

References

45. Amaya, D. J. et al. Marine heatwaves need clear definitions so coastal communities can adapt. *Nature* **616**, 29–32 (2023).
46. Pastor, F. & Khodayar, S. Marine heat waves: characterizing a major climate impact in the Mediterranean. *Sci. Total Environ.* **861**, 160621 (2022).
47. Sun, D., Jing, Z., Li, F. & Wu, L. Characterizing global marine heatwaves under a spatio-temporal framework. *Prog. Oceanogr.* **211**, 102947 (2022).
48. Gordon, A. D. *Classification* (CRC Press, 1999).
49. Sousa, P. M., Barriopedro, D., Garcia-Herrera, R., Woollings, T. & Trigo, R. M. A new combined detection algorithm for blocking and subtropical ridges. *J. Clim.* **34**, 7735–7758 (2021).
50. Pelly, J. L. & Hoskins, B. J. A new perspective on blocking. *J. Atmos. Sci.* **60**, 743–755 (2003).
51. D’Ortenzio, F. et al. Seasonal variability of the mixed layer depth in the Mediterranean Sea as derived from in situ profiles. *Geophys. Res. Lett.* **32**, L12605 (2005).
52. Bonino, G., Masina, S., Galimberti, G. & Moretti, M. Southern Europe and western Asia marine heat waves (SEWA-MHWs): a dataset based on macroevents. *Zenodo* <https://doi.org/10.5281/zenodo.7153255> (2022).
53. Good, S. A., Embury, O., Bulgin, C. E. & Mittaz, J. *ESA Sea Surface Temperature Climate Change Initiative (SST_cci): Level 4 Analysis Climate Data Record Version 2.1* (Centre for Environmental Data Analysis, 2019); <https://doi.org/10.5285/62c0f97b1eac4e0197a674870afe1ee6>
54. Copernicus Climate Change Service (C3S). *Sea Surface Temperature Daily Data from 1981 to Present Derived from Satellite Observations* (Copernicus Climate Change Service Climate Data Store, 2019); <https://doi.org/10.24381/cds.cf608234>
55. McAdam, R. & Bonino, G. Mediterranean summer marine heatwaves triggered by weaker winds under subtropical ridges: codes for analysis. *Zenodo* <https://doi.org/10.5281/zenodo.15690822> (2025).

Acknowledgements

G.B., R.M. and S.M. were supported by ObsSea4Clim ‘Ocean observations and indicators for climate and assessments’ funded by the European Union, grant agreement number: 101136548 (<https://doi.org/10.3030/101136548>) contribution number 11. E.S. was funded by the EU project BlueAdapt under grant agreement 101057764.

Author contributions

G.B., R.M., P.A., L.C., R.R.R., E.S., S.T. and S.M. conceived the study, provided critical input and assisted in interpretation of the results. G.B. and R.M. performed the analysis and wrote the paper. G.B., R.M., P.A., L.C., R.R.R., E.S., S.T. and S.M. reviewed and edited the paper.

Competing interests

The authors declare no competing interests.

Additional information

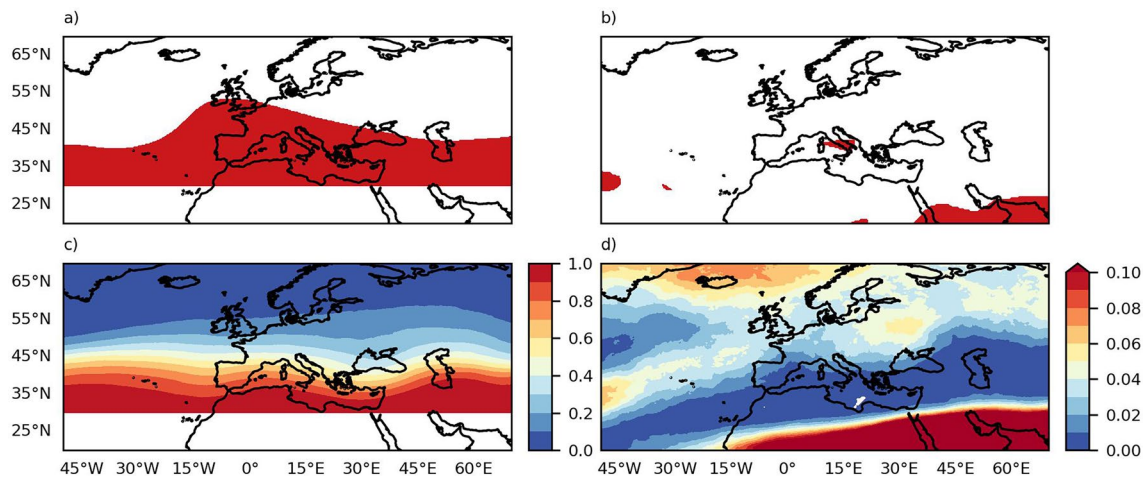
Extended data is available for this paper at <https://doi.org/10.1038/s41561-025-01762-9>.

Correspondence and requests for materials should be addressed to Giulia Bonino or Ronan McAdam.

Peer review information *Nature Geoscience* thanks Chaim Garfinkel, Dennis Hartmann and the other, anonymous, reviewer(s) for their

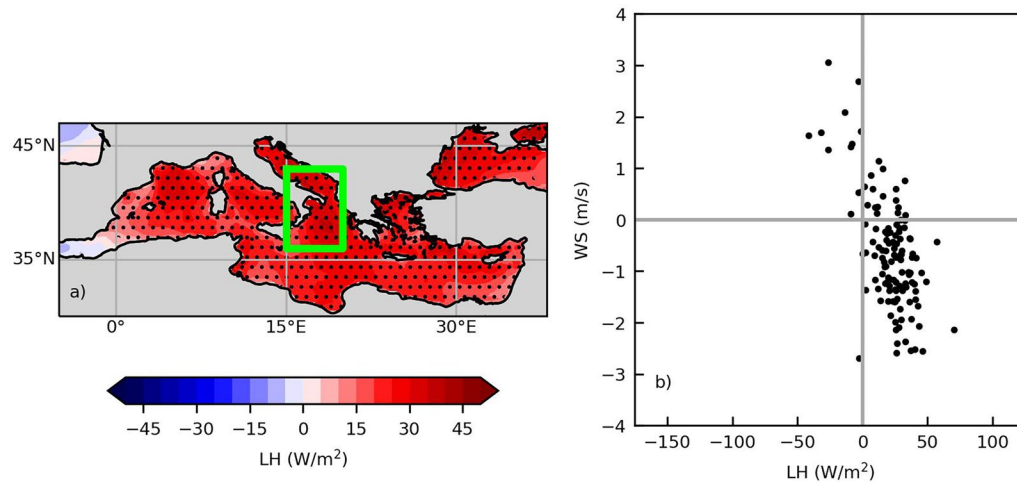
contribution to the peer review of this work. Primary Handling Editor: James Super, in collaboration with the *Nature Geoscience* team.

Reprints and permissions information is available at www.nature.com/reprints.

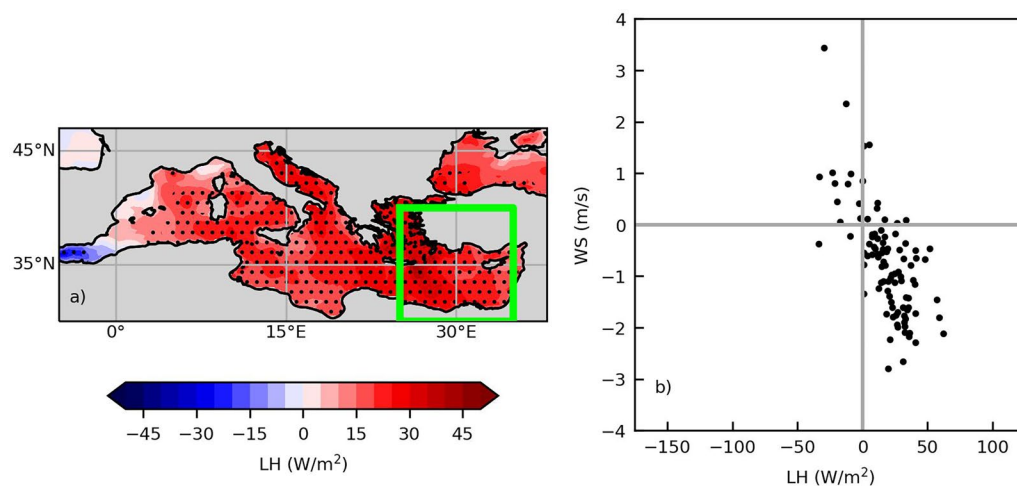


Extended Data Fig. 1 | Subtropical ridge and blocking indices. Subtropical ridge and blocking indices, applying the methods of Sousa et al.⁴⁹ and Rodrigues et al.³⁵ to ERA5 z500 and 2PV fields respectively. Example fields from 15th June 2003 for sub-tropical ridges (a) and blocking (b), where red displays

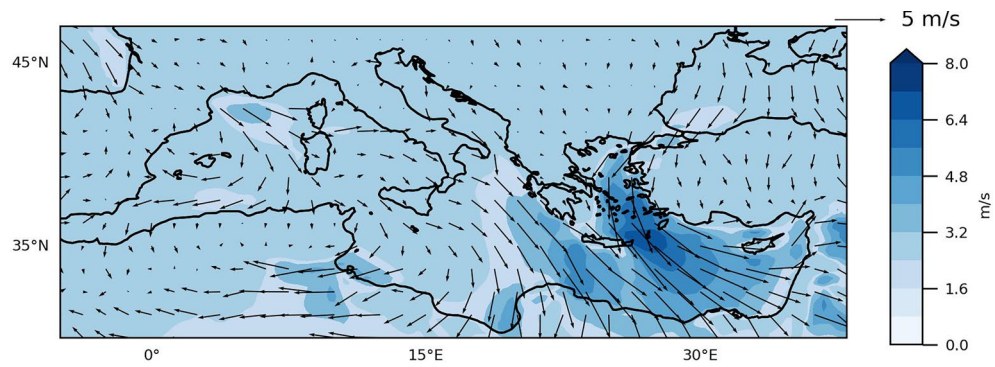
values of 1 (that is presence of ridge/blocking). Summer climatology from 1982–2022 of ridges (c) and blocking (d), equivalent to average occurrence (white indicates no occurrence on record). N.B The climatologies (c & d) have different colorbar scales. By definition, STRs occur poleward of 30°N.



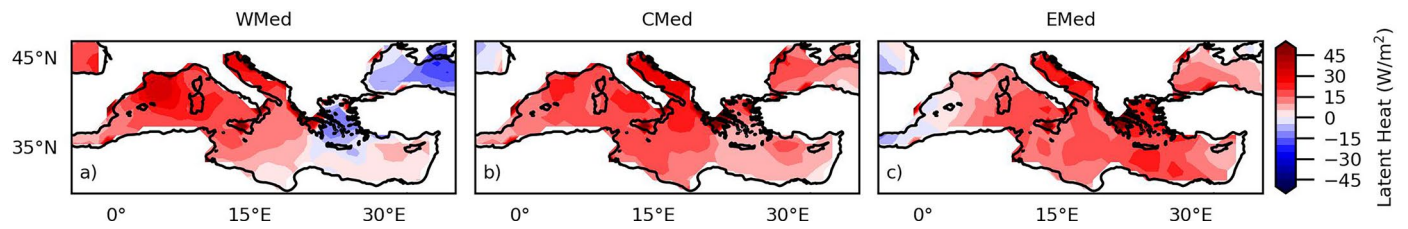
Extended Data Fig. 2 | CMed ERA5 wind speed and latent heat. ERA5 latent heat (LH; **a**) composites for CMed onset. Scatter plot of their daily anomalies during onset period (**b**); values are area-averages from green box in (**a**) and display a correlation equal to -0.65 . Black points **a** denote statistically significant anomalies (see bootstrapping in Methods).



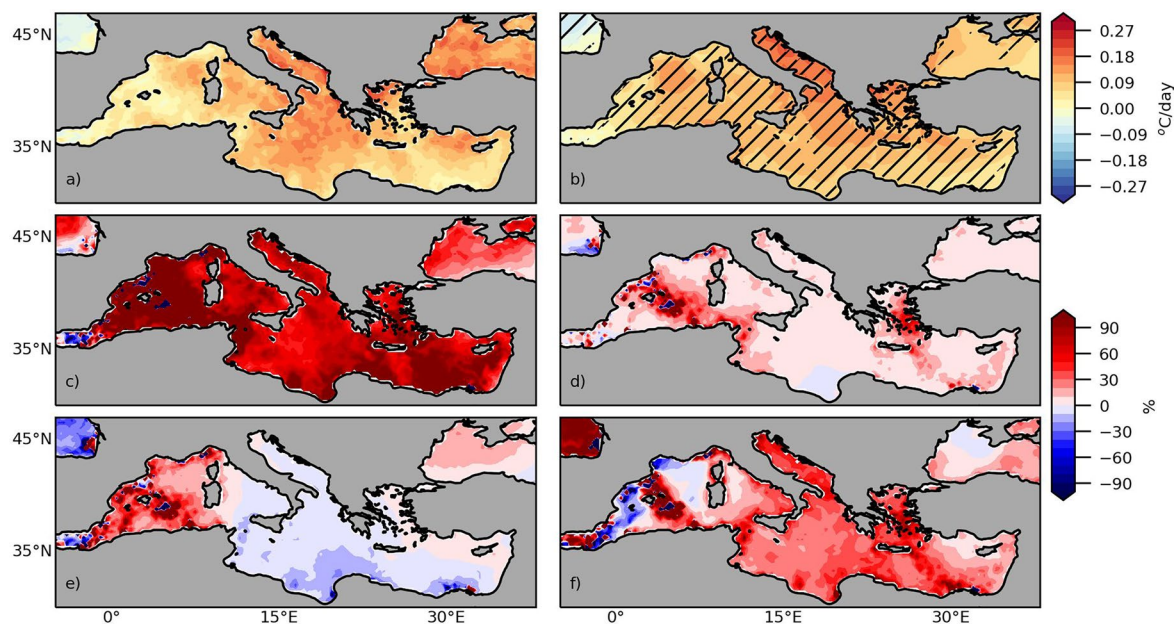
Extended Data Fig. 3 | EMed ERA5 wind speed and latent heat. As in Extended Data Fig. 2, but for EMed. Correlation between WS and LH is -0.69 .



Extended Data Fig. 4 | Climatology of ERA5 summer wind speed. Climatology of ERA5 summer wind speed and direction for the period 1982–2022, showing the northwesterly summer Mistrals (near 5°E, 40°N) and the northerly/northeasterly Etesians from 20°E to 35°E.

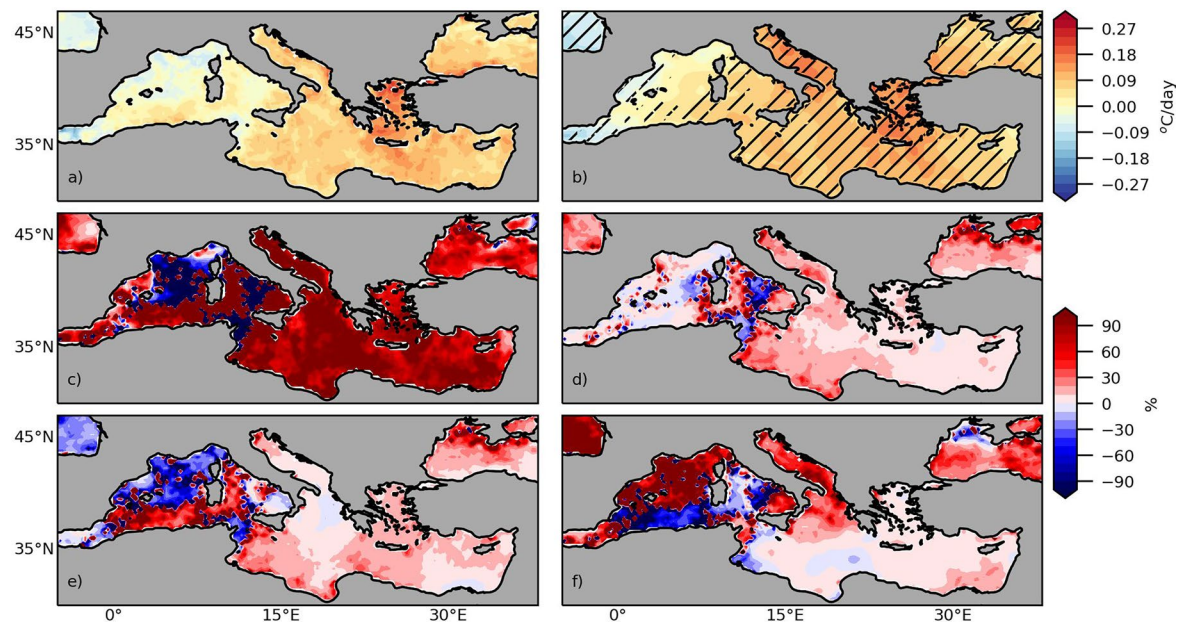


Extended Data Fig. 5 | Composites of latent heat flux in the observational OAFlux product. Composites of latent heat flux in the observational OAFlux product, for the three MHW clusters during MHW onset.

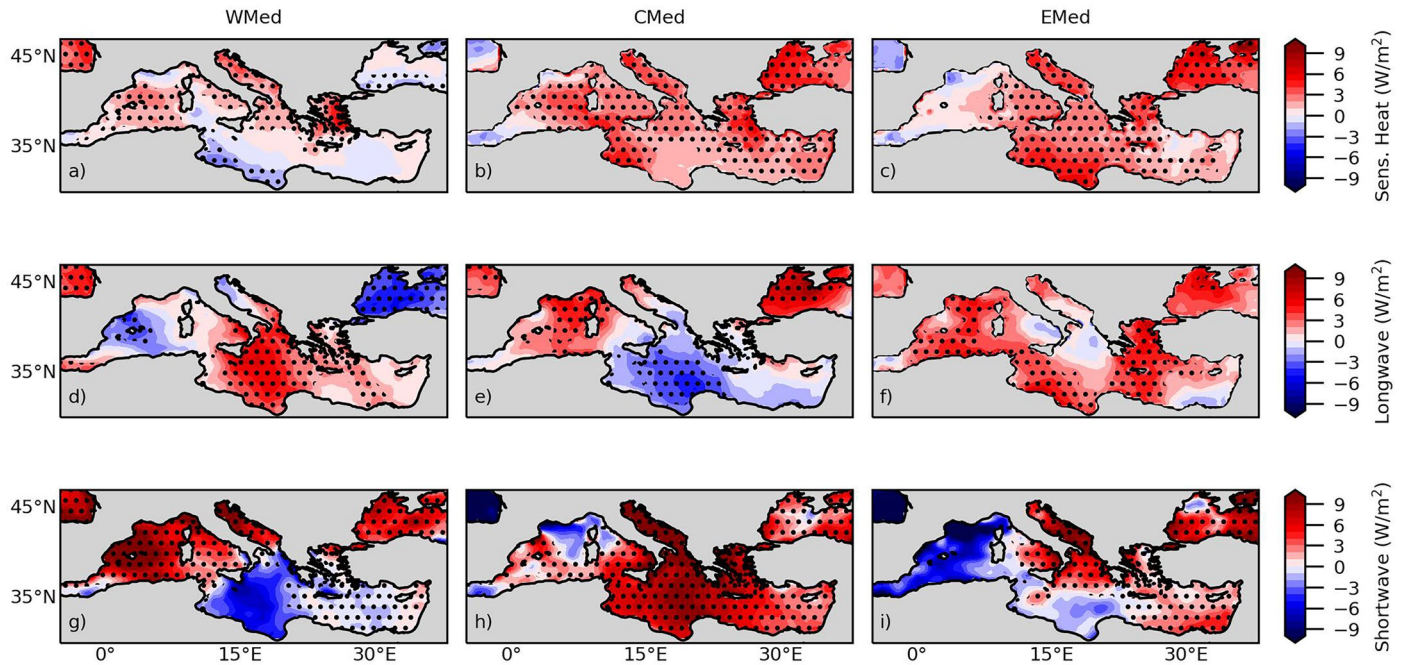


Extended Data Fig. 6 | CMed components of SST tendency. Composites of ESA CCI SST tendency (a), equivalent SST tendency of total fluxes (b) in CMed. Relative importance with respect to the SST tendency (a) of the four flux components in ERA5: Latent (c), sensible (d), longwave (e) and shortwave (f).

Hatching (in b) identifies where the equivalent flux tendency explains more than 70% of the SST tendency (in a). The anomalies are calculated against the full studied period (that is 1982–2022).



Extended Data Fig. 7 | Emed components of SST tendency. As in Extended Data Fig. 6, but for EMed.



Extended Data Fig. 8 | Composites of fluxes. Composites of sensible heat flux (a–c), longwave radiation (d–f) and shortwave radiation (g–i), in ERA5, for the three MHW clusters during MHW onset. Black points denote statistically significant anomalies (see bootstrapping in Methods). N.B the colorbar range is narrower with respect to the latent heat fluxes (Fig. 3 & Extended Data Fig. 5).